4-1-2008

Analysis of the Shaft Resistance of Nondisplacement Piles in Sand

Rodrigo Salgado
Purdue University, rodrigo@ecn.purdue.edu

Loukidis, D. & Salgado, R. (2008). *Géotechnique* **58**, No. 4, 283–296 [**doi:** 10.1680/geot.2008.58.4.283]

Analysis of the shaft resistance of non-displacement piles in sand

D. LOUKIDIS* and R. SALGADO

The paper examines, using numerical modelling, the problem of the limit shaft resistance of non-displacement piles installed in sands. The modelling makes use of an advanced, two-surface-plasticity constitutive model. The constitutive model predicts the soil response in both the small- and the large-strain range, while taking into account the effects of the intermediate principal effective stress and of the inherent anisotropy of the sand. Finite element analyses of shearing along the pile shaft are performed in order to examine the development of limit unit shaft resistance and the changes in stress state around the shaft upon axial loading of the pile. Special focus is placed on the operative value of the lateral earth pressure coefficient when limit shaft resistance is reached. The analyses offer useful insights regarding the factors controlling the value of unit shaft resistance in sands. The simulations predict a significant build-up of horizontal effective stress for dense sands. Based on these simulations, we propose a relationship between the lateral earth pressure coefficient for use in the calculation of the limit shaft resistance of the pile and the initial density and stress state of the sand.

KEYWORDS: constitutive relations; friction; numerical modelling and analysis; piles; plasticity; sands

La présente communication examine, au moyen de la modélisation numérique, le problème de la résistance limite de fût de pieu, dans les pieux sans déplacement installés dans le sable. La modélisation fait usage d'un modèle constitutif perfectionné de plasticité sur deux surfaces. Le modèle constitutif permet de prédire la réponse du sol dans des plages de déformation limitée et élevée, tout en tenant compte des effets des contraintes efficaces principales intermédiaires et de l'anisotropie inhérente du sable. On effectue des analyses aux éléments finis du cisaillement le long du fût du pieu afin d'examiner le développement de la résistance unitaire limite du fût, ainsi que les variations de la contrainte autour de l'arbre sous l'effet de l'application de charges axiales sur le pieu. On se concentre tout particulièrement sur la valeur opérative du coefficient de pression latérale de la terre lorsqu'on atteint la résistance limite du fût. Les analyses offrent un aperçu utile des facteurs déterminant la valeur de la résistance unitaire des fûts dans le sable. Les simulations permettent de prédire une accumulation significative de contraintes effectives horizontales pour les sables denses. Sur la base de ces simulations, nous proposons l'établissement d'un rapport entre le coefficient de pression latérale de la terre, pour le calcul de la résistance limite du fût, et la densité initiale et la contrainte du sable.

INTRODUCTION

In this paper we examine, using numerical analysis, the shaft resistance of non-displacement piles installed in sand. An ideal non-displacement pile is installed in the space left by soil previously removed without disturbing the surrounding soil or changing the stress state or density at any point of the surrounding soil. Drilled shafts (bored piles), which are non-displacement piles, induce some amount of disturbance very near the pile shaft when installed in a sandy profile. Nevertheless, disturbances are fairly small in properly executed drilling with the aid of bentonite or polymer slurry. According to Fleming *et al.* (1992), the placement of concrete with high fluidity would even lead to an initial K slightly greater than K_0. Thus we can assume that both the density and the stress state around a non-displacement pile after installation are the same as they are initially.

Given the relatively large permeability of sands and the generally low rate of application of the superstructure loads to the foundations, the limit unit shaft resistance q_{sL} can be calculated using drained analysis. The q_{sL} is the product of the normal effective stress on the soil/pile interface σ'_h and an appropriate friction coefficient μ_f ($= \tan\delta$). Because of the very large shear strains developed near the pile shaft at ultimate load levels, the value of friction angle δ mobilised in the vertical direction (parallel to the shaft wall) is expressed in terms of the constant-volume (or critical-state) friction angle ϕ_c. For non-displacement piles, given the high degree of roughness of the concrete placed in situ and the bonding between the soil particles at the borehole wall and the cement, the interlocking of the shaft with the soil is such that shearing will take place within the soil immediately adjacent to the pile (i.e. in a shear band running parallel and adjacent to the shaft wall), and not between the sand particles and the surface of the concrete shaft. The slurry has no effect on the shaft resistance since it is fully displaced by the concrete, provided that concrete is placed not long after excavation (Fleming *et al.*, 1992). Therefore the unit shaft resistance is controlled fully by the shear strength of the sand.

It is convenient in pile design to express σ'_h as the product of the initial (geostatic) vertical effective stress σ'_{v0} and an appropriate coefficient of lateral earth pressure K (Salgado, 2008). Therefore the unit limit shaft resistance can be written mathematically as

$$q_{sL} = K\sigma'_{v0}\tan\delta \tag{1}$$

The product $K\tan\delta$ is sometimes denoted by β, and the use of $\beta\sigma'_{v0}$ to compute q_{sL} is known as the 'β method'. Equation (1) is quite simple, but finding appropriate values for K, and consequently β, without proper analysis is rather difficult, a fact reflected in the wide range of values for K (and β) proposed in the literature. There have been relatively few studies proposing values for K or β or studying their dependence on the initial stress state and density of the sand, and these have been based on experimental results and back-analyses of pile load test results. The present paper sheds

Manuscript received 2 July 2006; revised manuscript accepted 23 January 2008.
Discussion on this paper closes on 1 November 2008, for further details see p. ii.
* School of Civil Engineering, Purdue University, W. Lafayette, USA.

light on this issue through numerical simulations using an advanced constitutive model and the finite element method.

METHODOLOGY OF NUMERICAL SIMULATION

General concepts and deformation mechanism

Let us first examine the mode of deformation and stress conditions developed in a soil element in contact with the pile shaft (the very first element in a row of elements extending all the way from the pile shaft wall to infinity). This element is not near either the pile tip or the ground surface. Let us also assume that there is no development of normal strain in the vertical direction at any moment ($\dot{\varepsilon}_z = 0$). As the pile is subjected to axial loading, the soil element under consideration will be subjected to a mode of shear loading that involves stress rotation, with the major and minor principal effective stresses tending to an inclination of $\pm 45°$ with the vertical as shearing proceeds. If the soil is generally dilative, then elements closer to the pile push against their neighbouring soil elements lying in the same horizontal plane but located further away from the pile, a process that leads to the build-up of lateral effective stress. In general, the mode of deformation is not strictly that of simple shear, as the change in soil volume leads to both radial and hoop strains (Fig. 1). After a certain amount of vertical pile displacement, the soil close to the pile reaches critical state (CS), stops dilating, and the shaft resistance reaches its limiting value. This mechanism is similar to the normal stress build-up in experimental studies employing constant-normal-stiffness direct shear tests (e.g. Boulon & Foray, 1986; Tabucanon *et al.*, 1995).

Constitutive model

There are certain characteristics that a constitutive model must possess in order for it to be able to simulate the shaft shearing process described in the previous section. These are: (a) the ability to predict the critical state; (b) the ability to produce the correct soil stiffness at small and large strains; and (c) the ability to simulate sand behaviour under conditions other than triaxial compression/extension. For accurate simulations of any loading path, the model must take into account the effect of the intermediate effective stress and the effect of fabric-related (inherent) cross-anisotropy. Inherent cross-anisotropy results from the fact that the prevalent direction of the long axis of sand particles deposited under the action of gravity through water or air is perpendicular to the axis of deposition (vertical axis).

The constitutive model we use in this paper was originally proposed by Manzari & Dafalias (1997) (Fig. 2). It combines a number of features from subsequent work by Li & Dafalias (2000), Papadimitriou & Bouckovalas (2002), Dafalias & Manzari (2004) and Dafalias *et al.* (2004), along with new additions and improvements. The model has been calibrated for dry-deposited/air-pluviated Toyoura sand based mainly on data from triaxial tests (Fukushima & Tatsuoka, 1984; Yoshimine *et al.*, 1998), plane-strain biaxial tests (Lam & Tatsuoka, 1988), and hollow cylinder tests (Yoshimine *et al.*, 1998). Model parameters have been also determined for slurry-deposited/water-pluviated Ottawa sand based on test data by Carraro *et al.* (2003), Carraro (2004), and Murthy *et al.* (2007). Toyoura sand is an angular to sub-angular silica sand with $D_{50} = 0{\cdot}19$ mm, $e_{min} = 0{\cdot}60$ and $e_{max} = 0{\cdot}98$. Ottawa sand is a round to sub-round silica sand with $D_{50} = 0{\cdot}39$ mm, $e_{min} = 0{\cdot}48$ and $e_{max} = 0{\cdot}78$. The model is compatible with the framework of critical-state soil mechanics, taking the inherent anisotropy of sands into account through the use of a fabric tensor (Dafalias *et al.*, 2004). It reproduces the soil response over the entire range

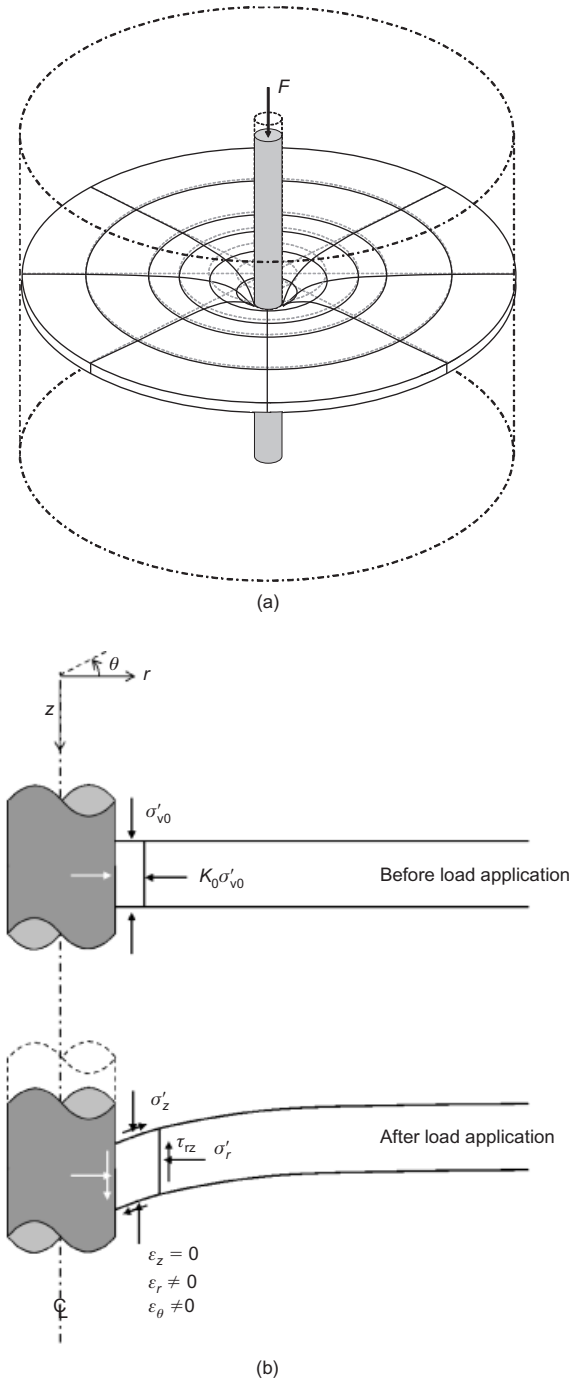

Fig. 1. (a) Idealised deformation pattern around pile; (b) stress and deformation conditions for soil elements adjacent to pile shaft upon application of axial load

of strains, with initial shear modulus equal to G_{max}, as measured in resonant column or bender elements tests, and with a realistic value of the small-strain Poisson's ratio ν (= 0·1–0·2). This feature is particularly desirable because elements far away from the shaft will develop only small shear strains, but they will still resist the deformation of the elements closer to the shaft. The equations of the constitutive model and the values of its input parameters can be found in Tables 1 and 2 respectively. Model equations that we have modified are shown shaded in Table 1. Detailed information about the calibration of the model parameters and the performance of the model in predicting the sand response observed in laboratory tests can be found in Loukidis (2006) and Loukidis & Salgado (2008). Compari-

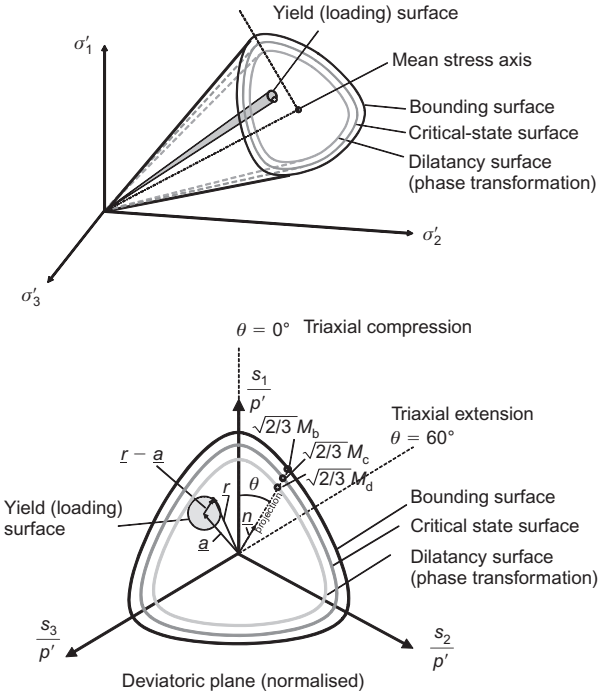

Fig. 2. Schematic representation of two-surface plasticity constitutive model in general stress space

sons between constitutive model predictions and experimental data from drained triaxial compression tests on Toyoura sand (Fukushima & Tatsuoka, 1984) and clean Ottawa sand (Carraro, 2004) are shown in Fig. 3.

Finite element model

Potts & Martins (1982) used finite elements (FE) to investigate the pile shaft resistance in clays under drained conditions. They assumed that end conditions do not influence the development of limit shaft resistance at depths well away from both the ground surface and the pile base, and that the vertical normal strain rate will be very small or zero. This idealisation allows modelling using just a thin disc of soil that is allowed to experience only vertical shearing and radial expansion or contraction. Consequently the problem becomes independent of scale in the vertical direction, and reduces to a one-dimensional axisymmetric problem. Use of rectangular elements (instead of triangular elements), in addition to imposition of these deformation constraints, renders the solution completely independent of the height of the elements. The same formulation can be seen also as simulating the shearing of a cavity of infinite vertical extent. An analysis of a soil disc can give useful insights into the fundamental mechanics controlling shaft resistance in sand (Salgado, 2006), without the complexities present in the full (two-dimensional axisymmetric) pile simulation.

In the one-dimensional axisymmetric simulations, the mesh consists of a single row of 125 to 500 elements. Referring to Fig. 4, at the leftmost boundary (where the pile/soil interface is), the vertical displacement is applied in small increments (of the order of 10^{-7} to 10^{-6} of the pile diameter B for the results to converge to an accurate solution), while the horizontal displacement is kept to zero. Given the extremely large stiffness of concrete compared with that of soil, the pile is assumed to be perfectly rigid, and is not included in the mesh. The boundary conditions for the one-dimensional simulations are shown in Fig. 4. Nodes lying in the same vertical are tied together with respect to both vertical and horizontal movement, as done by Gens & Potts (1984). This means that the distortion of the soil as the pile is pushed down is captured by vertical shearing of the elements, which can neither rotate nor contract/stretch in the vertical direction. The elements are still able to contract or stretch in the radial direction.

We also performed a number of two-dimensional axisymmetric analyses of a pile of finite length, whose results we compared with those of the one-dimensional analyses. In reality, and in contrast with the one-dimensional approach, the initial overburden stress varies with depth and, kinematically, the soil elements can elongate or contract in the vertical direction. Additionally, downdrag of the soil by the pile as it moves down is constrained to some extent by the presence of the soil lying at depths lower than the pile tip. This leads to an oblique (conical) transfer of stresses (arching) (Touma & Reese, 1974), which is illustrated in Fig. 5. In the full-pile (two-dimensional axisymmetric) simulations, we apply the same displacement increments along the entire pile/soil interface, including the pile tip, assuming a perfectly rigid pile. In contrast to the one-dimensional simulations, the degrees of freedom in the two-dimensional simulations are not tied. The mesh and boundary conditions used for the two-dimensional simulation are shown in Fig. 6.

The constitutive model was implemented in the finite element program SNAC (Abbo & Sloan, 2000). Eight-noded quadrilateral, axisymmetric elements are used to discretise the analysis domain. The integration of the stress–strain equations at the Gauss quadrature points is done using the semi-implicit backward-Euler (cutting plane) algorithm adapted with sub-incrementation and error control (Abbo & Sloan, 2000; Loukidis, 2006). This algorithm has compared favourably (both in accuracy and in efficiency) with the Runge–Kutta–Dormand–Prince sub-stepping algorithm (Sloan & Booker, 1992). The stress error tolerance and the yield function error tolerance were set to be 10^{-4} and 10^{-9} respectively. The global load incrementation scheme used was the modified Newton–Raphson scheme with the global stiffness matrix being always the elastic stiffness matrix. This choice was based on the fact that the high degree of non-associativity and strain-softening present in the constitutive model give rise to considerable difficulties in the inversion of the elasto-plastic global stiffness matrix used in the original Newton–Raphson scheme, which becomes ill-conditioned.

Shear strain is highly localised next to the pile shaft, along which a shear band forms. It is well known that, in FE analyses involving a strain-softening material, the problem of solution non-uniqueness may arise, leading to physically irrelevant solutions. Because the shearing tends to concentrate within the elements where softening starts, the predicted shear band thickness becomes unrealistically small as the element size in the softening region decreases with successive mesh refinements. Various experimental studies (e.g. Uesugi *et al.*, 1988; Vardoulakis & Sulem, 1995; Nemat-Nasser & Okada, 2001) on shear strain localisation in sand have shown that the shear band thickness t_s is in the range of 5 to $20D_{50}$. Most soil constitutive models, including the one we use in this paper, describe soil behaviour as if soil were a continuum. They are not intended to and cannot capture the mechanics of subsets of the shear band: therefore we must not have elements smaller (thinner) than the shear band.

Strategies to deal with the problem of non-uniqueness of solutions include the use of regularisation techniques, such as the Cosserat continuum, gradient-dependent plasticity, and non-local plasticity. These techniques introduce explicitly or implicitly an internal length scale that helps the analysis converge to a finite and realistic shear band thickness.

Table 1. Equations of two-surface plasticity constitutive model.

Description	Equation number	Constitutive equations	Parameters	References/notes
Stress–strain relations	(2)	$\dot{\sigma}'_{ij} = 2G(\dot{\varepsilon}_{ij} - \dot{\varepsilon}^{\mathrm{p}}_{ij}) + (K - \frac{2}{3}G)(\dot{\varepsilon}_{kk} - \dot{\varepsilon}^{\mathrm{p}}_{kk})$	–	–
Small-strain shear modulus	(3)	$G_{\max} = C_{\mathrm{g}} \dfrac{(2{\cdot}17 - e)^2}{1+e} p'^{\,n_{\mathrm{g}}} \cdot p_{\mathrm{A}}^{1-n_{\mathrm{g}}}$	C_{g}, n_{g}	Hardin & Richart (1963)
Elastic shear modulus with Ramberg–Osgood degradation	(4)	$G = \dfrac{G_{\max}}{1 + 2\left(\dfrac{1}{\alpha_1} - 1\right)\left[\dfrac{\sqrt{3/2}\sqrt{(r_{ij} - a_{ij,\mathrm{ini}})(r_{ij} - a_{ij,\mathrm{ini}})}}{2\alpha_1 (G_{\max}/p')\gamma_1}\right]} \geqslant \dfrac{G_{\max}}{1 + 2\left(\dfrac{1}{\alpha_1} - 1\right)}$	α_1, γ_1	Papadimitriou & Bouckovalas (2002)
Elastic bulk modulus	(5)	$K = \dfrac{2(1+\nu)}{3(1-2\nu)} G$	ν	–
Yield (loading) surface	(6)	$f = \sqrt{(s_{ij} - a_{ij}p')(s_{ij} - a_{ij}p')} - \sqrt{\frac{2}{3}} m \cdot p' = 0$	m	Manzari & Dafalias (1997)
Plastic multiplier	(7)	$\dot{\Lambda} = \dfrac{1}{H}[n_{ij} - \frac{1}{3}(n_{kl} r_{kl}) \cdot \delta_{ij}]\dot{\sigma}'_{ij}$ where $n_{ij} = (r_{ij} - a_{ij}) / \sqrt{(r_{ij} - a_{ij})(r_{ij} - a_{ij})}$ and $r_{ij} = s_{ij}/p'$	–	Manzari & Dafalias (1997)
Bounding, dilatancy and CS surfaces	(8a), 8(b), 8(c)	$M_{\mathrm{b}} = g(\theta) \cdot M_{\mathrm{cc}} \exp(-k_{\mathrm{b}} \cdot \psi)$, $M_{\mathrm{d}} = g(\theta) \cdot M_{\mathrm{cc}} \exp(k_{\mathrm{d}} \cdot \psi)$, $M_{\mathrm{c}} = g(\theta) \cdot M_{\mathrm{cc}}$	M_{cc}, k_{b}, k_{d}	Li & Dafalias (2000)
State parameter and CSL in e–p'	9(a), 9(b)	$\psi = e - e_{\mathrm{c}}$, $e_{\mathrm{c}} = \Gamma - \lambda \cdot \left(\dfrac{p'}{p_{\mathrm{A}}}\right)^{\xi}$	λ, ξ	Li *et al.* (1999)
Shape of bounding, dilatancy, CS surfaces in the π plane	(10)	$g(\theta) = \dfrac{2^{n_{\mathrm{s}}} c_1}{[1 + c_1^{1/n_{\mathrm{s}}} - (1 - c_1^{1/n_{\mathrm{s}}})\cos(3\theta)]^{n_{\mathrm{s}}}}$	c_1, n_{s}	Modified expression
Plastic modulus	11(a), 11(b)	$H = h_0 \cdot h_k \sqrt{\dfrac{2}{3}} \cdot \dfrac{G \cdot \exp(k_{\mathrm{b}}\psi) \cdot \left[\sqrt{\frac{2}{3}}(M_{\mathrm{b}} - m) - a_{ij} n_{ij}\right]}{\left[\sqrt{\frac{3}{2}}\sqrt{(r_{ij} - a_{ij,\mathrm{ini}})\ (r_{ij} - a_{ij,\mathrm{ini}})}\right]^{\mu}}$, $h_0 = \left(\dfrac{e_{\lim} - e}{h_2}\right)^{h_1}$	h_1, h_2, $e_{\lim}$, μ	Modified expression for h_0 Addition of exponent μ
Flow rule	(12a), (12b) (12c)	$\dot{\varepsilon}^{\mathrm{p}}_{ij} = \dot{\Lambda} \cdot (R'_{ij} + \frac{1}{3} D\delta_{ij})$, $R'_{ij} = R'^{*}_{ij} / \sqrt{R'^{*}_{ij} R'^{*}_{ij}}$ $R'^{*}_{ij} = \left[1 + \dfrac{3}{2}\left(\dfrac{1-c_2}{c_2}\right) g_2(\theta)\cos(3\theta)\right] n_{ij} - \left[3\sqrt{\dfrac{3}{2}}\left(\dfrac{1-c_2}{c_2}\right) g_2(\theta)\right] \cdot \left(n_{ik} n_{kj} - \dfrac{1}{3}\delta_{ij}\right)$	c_2	Dafalias & Manzari (2004) Normalisation of R'^{*}_{ij}

Dilatancy	(13)	$D = \frac{D_o}{M_{cc}} \cdot \left[\sqrt{\frac{2}{3}}(M_d - m) - a_{ij} n_{ij}\right]$	D_o	Manzari & Dafalias (1997)
Shape of plastic potential in π plane	(14)	$g_2(\theta) = \frac{2c_2}{(1+c_2) - (1-c_2)\cos(3\theta)}$	c_2	$c_2 \neq c_1$
Fabric tensor	(15)	$F_{11} = F_{33} = 0{\cdot}5(1-\alpha),\ F_{22} = \alpha$	α	Dafalias *et al.* (2004)
Fabric dependent scalar	(16)	$F_{ij} = 0$ for $i \neq j$ $A_f = g(\theta)[F_{ij} n_{ij}]$	–	Dafalias *et al.* (2004)
Fabric effect multiplier in H	(17a), (17b)	$h_k = \exp\{[(A_{fc} - A_f)/(A_{fc} - A_{fe})]^{1{\cdot}25} \cdot \ln(k_h)\},\ A_{fc} = -(1/c_1)A_{fe} = \sqrt{\frac{3}{2}}(\alpha - \frac{1}{3})$	k_h	Modified h_k expression
Intercept of CSL	(18)	$\Gamma = \Gamma_c \cdot \exp(A_{fc} - A_f)$	Γ_c	CSL in TXC is independent of fabric
Kinematic hardening of yield surface	(19)	$\dot{a}_{ij} = \dot{\Lambda} \cdot \frac{H}{p'} \cdot \frac{\sqrt{\frac{2}{3}}(M_b - m) n_{ij} - a_{ij}}{\sqrt{\frac{2}{3}}(M_b - m) - a_{ij} n_{ij}}$	–	Manzari & Dafalias (1997)

G, current value of shear modulus; K, bulk modulus; H, plastic modulus; σ'_{ij}, effective stress tensor; s_{ij}, deviatoric stress tensor; p', mean effective stress; a_{ij}, kinematic hardening tensor; $a_{ij,ini}$, initial value of kinematic hardening tensor; δ_{ij}, Kronecker's delta; ε_{ij}, strain tensor; Λ, plastic multiplier; ε^p_{ij}, plastic strain tensor.
Note: equations revised by the authors are shaded.

However, these techniques introduce a variety of complexities into the FE formulation, and usually require significant alterations or additions to the constitutive model (especially the first two techniques). In the present analysis, the issue of non-uniqueness is dealt with in a much simpler way, which is possible and practical because we know *a priori* the exact location and orientation of the shear band (which is parallel and adjacent to the sand/concrete interface). We set the size (width) of elements right at the contact with the boundary representing the pile shaft to be equal to the shear band thickness t_s that would be observed in reality, in both the one-dimensional and two-dimensional simulations. In this way we implicitly assume that the vertical sides of the leftmost element correspond to the boundaries of the shear band. So most of the analyses were done for a minimum element size (size of leftmost element) of $10D_{50}$, corresponding to approximately 2 mm for Toyoura sand and 4 mm for Ottawa sand. It should be noted that neither t_s nor D_{50} is a parameter of the constitutive model; they both enter the analysis at the level of the boundary-value problem.

RESULTS AND DISCUSSION

One-dimensional analysis (analysis using a soil disc)

Figure 7 shows the evolution of the shear stress τ_s and normal stress σ'_n on the left boundary (the pile/soil interface) that develops with increasing vertical pile displacement for the case of $\sigma'_{v0} = 100$ kPa, relative density $D_R = 60\%$ and $K_0 = 0{\cdot}4$. The pile diameter B is 0·5 m. The shear and normal stresses τ_s and σ'_n are derived from the vertical and horizontal reactions at the nodes of the left boundary respectively. The shear stress increases non-linearly with displacement until a peak (failure) point, and then drops to the steady value of q_{sL} we seek. The value of pile movement w_L required for mobilisation of q_{sL} in this case is of the order of 5 mm (or about 1% of the pile diameter).

The softening response, shown in Fig. 7(a), is rather abrupt. This is a consequence of the intense shear strain localisation. The initiation of the softening corresponds to the formation of the shear band along the pile/soil interface, and deformation is localised in the leftmost element (Fig. 7(c)). Unloading occurs in other elements that are in the vicinity of the element representing the shear band after reaching peak resistance. Fig. 8 shows the stress path for the Gauss quadrature point closest to the pile in the normalised deviatoric plane (where principal deviatoric stresses s_1, s_2, and s_3 are normalised with respect to mean effective stress p', and the deviatoric plane is scaled by a factor equal to $\sqrt{3/2}$ so that the radial distance in triaxial compression and extension is equal to the stress ratio used in geomechanics). According to the definition used in this paper, Lode's angle θ takes the value of 0° for triaxial compression and 60° for triaxial extension. It can be seen that the stress path starts from the geostatic stress state, for which $\theta = 0°$ (corresponding to $b = (\sigma'_2 - \sigma'_3)/(\sigma'_1 - \sigma'_3) = 0$), proceeds to higher θ values until the peak state, and then softens towards critical state (CS). At CS, Lode's angle θ becomes equal to 14·4°, which corresponds to a b value of 0·26. This value of b is virtually identical to the value of b at CS under plane-strain conditions for Toyoura sand (Pradhan *et al.*, 1988; Yoshimine *et al.*, 1998). The b value at CS under plane-strain conditions is controlled by the shape of the plastic potential (equation for $g_2(\theta)$ in Table 1) in the deviatoric plane (Potts & Zdravković, 1999; Dafalias *et al.*, 2004) through the value of the model parameter c_2 (Table 2). The mode of deformation of the soil in the thin zone surrounding the pile is almost identical to simple shear, which is a special case of plane strain. The near identity to simple shear (SS) conditions can be understood by the fact that the ratio

Table 2. Constitutive model input parameters.

	Parameter symbol	Parameter value		Test data required
		Toyoura sand (dry-deposited/ air-pluviated)	Ottawa sand (slurry-deposited/ water-pluviated)	
Small-strain ('elastic') parameters	ν	0·15	0·15*	Tests using local strain transducers or isotropic compression or 1-D compression tests with unloading path
	C_g	900	611	Bender element or resonant column tests
	n_g	0·400	0·437	Bender element or resonant column tests
	γ_1	0·0010	0·00065	Resonant column tests or TX tests with local strain measurements
	α_1	0·40	0·47	Undrained TX compression tests
Critical state	Γ_c	0·934	0·780	TX compression tests
	λ	0·019	0·081	TX compression tests
	ξ	0·70	0·20	TX compression tests
	M_{cc}	1·27	1·21	TX compression tests
Bounding surface	k_b	1·5	1·9	TX compression tests
Dilatancy	D_o	0·90	1·31	TX compression tests
	k_d	2·8	2·2	TX compression tests
Plastic modulus	h_1†	1·62	2·20	TX compression tests
	h_2†	0·254	0·240	TX compression tests
	e_{lim}†	1·00	0·81	TX compression tests
	μ†	2·0	1·2	Undrained TX compression tests
Stress-induced anisotropy	c_1	0·72	0·71	TX extension tests
	c_2	0·78	0·78*	SS or other plane-strain tests
	n_s	0·35	0·35*	SS or other plane-strain tests
Inherent (fabric) anisotropy	α	0·29	0·31	TX extension tests
	k_h†	0·11	0·39	TX extension tests
Yield surface radius	m	0·05	0·05	

* Assumed.
† Parameters determined based on trial and error simulations; all other parameters are determined directly from experimental data.

of the hoop strain rate $\dot{\varepsilon}_\theta$ to the radial strain rate $\dot{\varepsilon}_r$ for the leftmost element with thickness t_s is of the same order as the ratio t_s/R (0·008 in the present case), where R is the pile radius, yielding an $\dot{\varepsilon}_\theta$ two orders of magnitude less than $\dot{\varepsilon}_r$.

At the initial state, the major principal effective stress is vertical (since $K_0 < 1$) and equal to σ'_{v0}. As vertical shear progresses, σ'_1 and σ'_3 rotate, and, at CS, they form an angle of $\pm 45°$ with the vertical (the vertical and radial normal stresses become equal). This is consistent with observations of SS tests on Toyoura sand by Pradhan *et al.* (1988) and Yoshimine *et al.* (1998). The true (maximum obliquity) friction angle at CS, ϕ_c $(= \sin^{-1}[(\sigma'_1 - \sigma'_3)/(\sigma'_1 + \sigma'_3)])$, inside the soil under these conditions is 36·6° (Fig. 8), which is consistent with the value of the CS friction angle for plane strain conditions ϕ_c^{PS} for Toyoura sand (Lam & Tatsuoka, 1988; Pradhan *et al.*, 1988; Yoshimine *et al.*, 1998). The friction angle δ $(= \tan^{-1}(\tau_s/\sigma'_n))$ mobilised on the left boundary along the vertical direction (parallel to the pile shaft/soil interface) at the state of limit shaft resistance turns out to be equal to 30·8° (corresponding to $\mu_f = 0·6$) in all analyses involving a t_s in the range of $5D_{50}$ to $20D_{50}$. This value is in very good agreement with the residual (constant-volume) friction coefficient from interface simple shear tests on Toyoura sand by Uesugi *et al.* (1990). The ϕ_c angle does not mobilise along the vertical plane; it in fact mobilises in a plane that is inclined by an angle approximately equal to $\phi_c/2$ with respect to the vertical. The friction angles δ and ϕ_c under SS conditions are related through the equation (Potts & Martins, 1982):

$$\delta = \tan^{-1}(\sin\phi_c) \tag{20}$$

The values of ϕ_c (36·6° for plane strain) and δ (30·8°) resulting from the analysis satisfy equation (20). The critical-state friction angle of Toyoura sand for triaxial compression conditions ϕ_c^{TXC} is 31·6°. Comparing the values of δ and ϕ_c^{TXC}, we can conclude that an operative value for δ can be considered to be $0·97\phi_c^{TXC}$ (from analyses with Ottawa sand, $\delta = 0·98\phi_c^{TXC}$).

From the ratio of the normal stress acting on the shaft at the limit state to σ'_{v0}, we can obtain the value of K. The K/K_0 for different values of initial D_R and σ'_{v0} are plotted in Fig. 9(a). In this set of runs, the coefficient of earth pressure at rest, K_0, was set equal to 0·4 and the pile diameter, B, was 0·5 m. In general, for sand that has not experienced larger overburden stress than its current value, we expect K_0 to be in the range of 0·4 to 0·5 (Mesri & Hayat, 1993). K increases with D_R and decreases with increasing σ'_{v0}. These trends reflect the effect of sand dilatancy on the build-up of lateral effective stress upon shearing. The analyses yield K less than K_0 for 30% relative density and large effective stress. On the other hand, K can be as high as $2·5K_0$ for $D_R = 90\%$ and $\sigma'_{v0} = 50$ kPa. The value of σ'_{v0} impacts strongly on the value of pile settlement required for reaching limit shaft resistance conditions w_L. From the Toyoura sand analyses shown in Fig. 9(a), the average w_L value is 4·4 mm, 6·3 mm, 7·8 mm, and 10·2 mm for σ'_{v0} equal to 50 kPa, 100 kPa, 200 kPa and 500 kPa respectively. The limiting settlement w_L is an increasing function of the sand shear strength (τ_f) and a decreasing function of G_{max}. Because the sand strength is almost proportional to σ'_{v0}, whereas G_{max} is a power function of σ'_{v0} with an exponent that is much less than 1 (0·4 for Toyoura sand), the net outcome is an increase in w_L with increasing σ'_{v0}. This is consistent with observations from model plate pull-out tests by Garnier & König (1998) and constant normal stress interface shear tests by

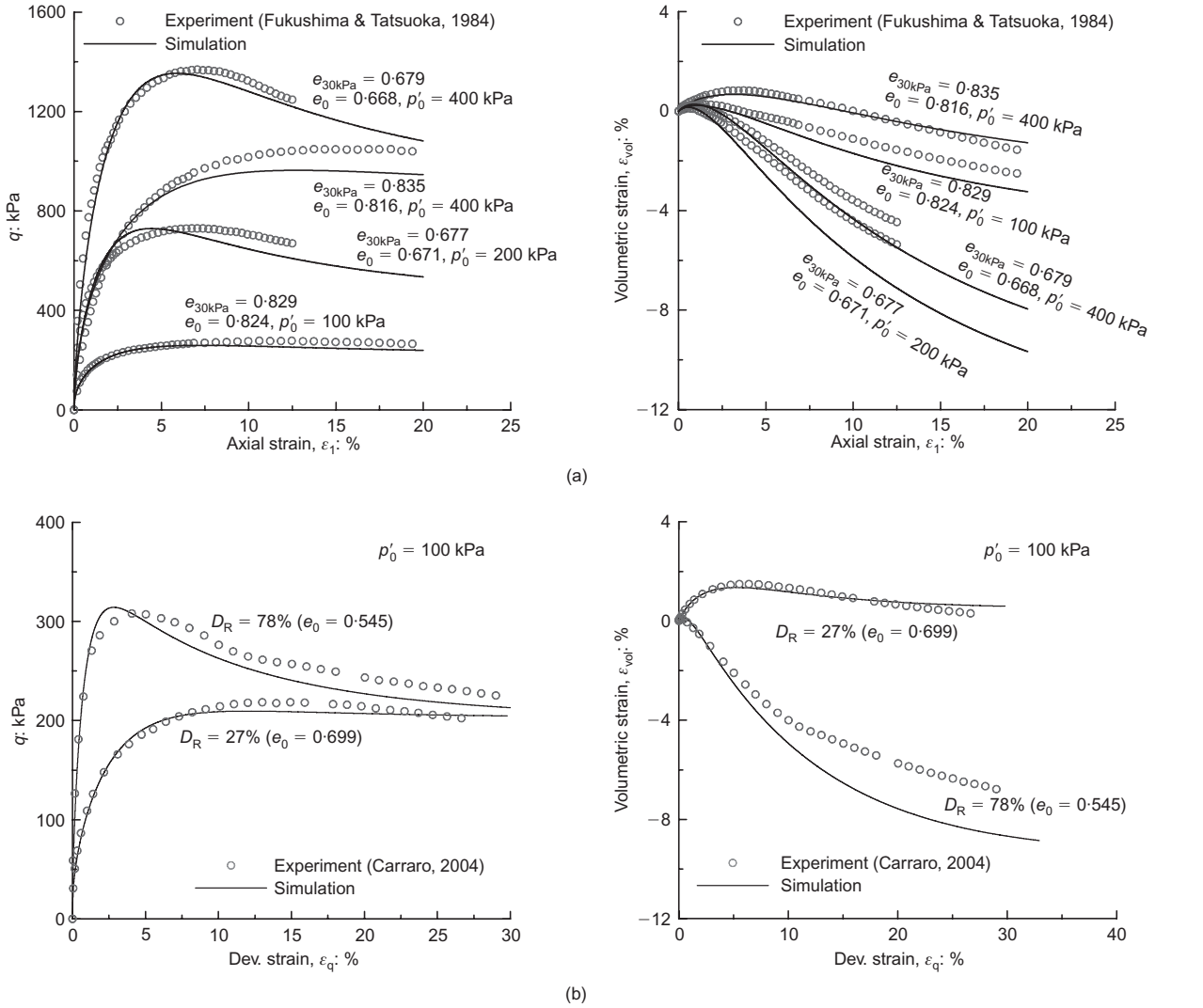

Fig. 3. Drained triaxial compression tests on (a) air-pluviated Toyoura sand and (b) clean Ottawa sand: model predictions and experimental data

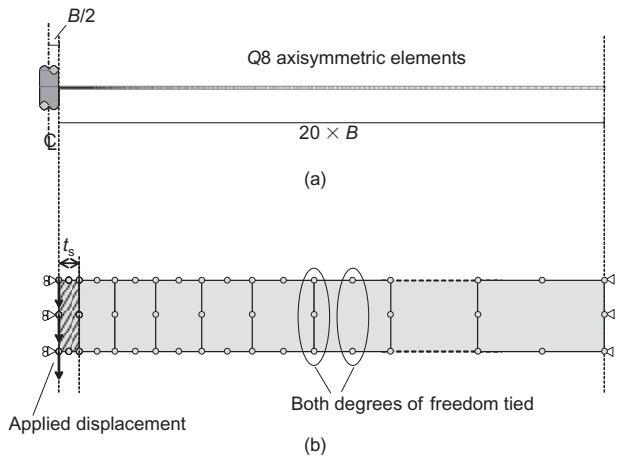

Fig. 4. (a) Finite element mesh and (b) boundary conditions and constraints used in one-dimensional simulations

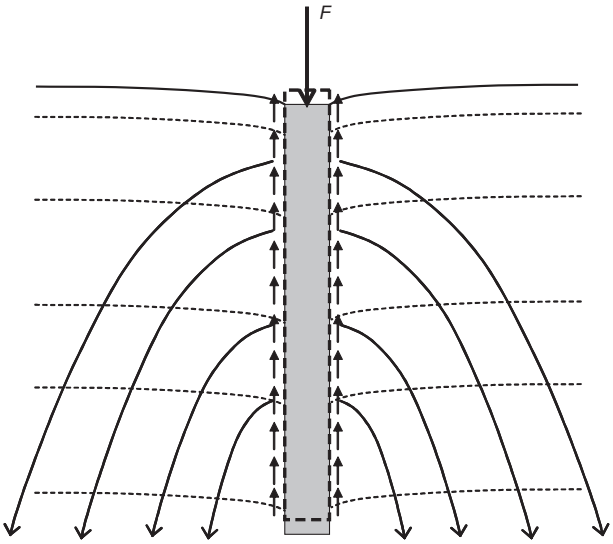

Fig. 5. Schematic of stress transfer (arching) in the case of a pile loaded axially in compression

Ghionna & Mortara (2002). Fig. 9(a) shows that the K/K_0 for sand is smaller for Ottawa than for Toyoura. This suggests that, for a given value of relative density, Ottawa sand has a smaller potential for dilation and normal stress build-up than Toyoura sand; this can be attributed to the fact that Ottawa sand has rounded to sub-rounded particles, whereas Toyoura sand is a sub-angular to angular sand.

A set of simulations was performed with K_0 = 0·4, 0·5 (for the case of normally consolidated sands), 1·0 and 2·0 (representing heavily overconsolidated sands) and σ'_{v0} = 100 kPa (Fig. 9(b)). The potential for lateral stress build-up

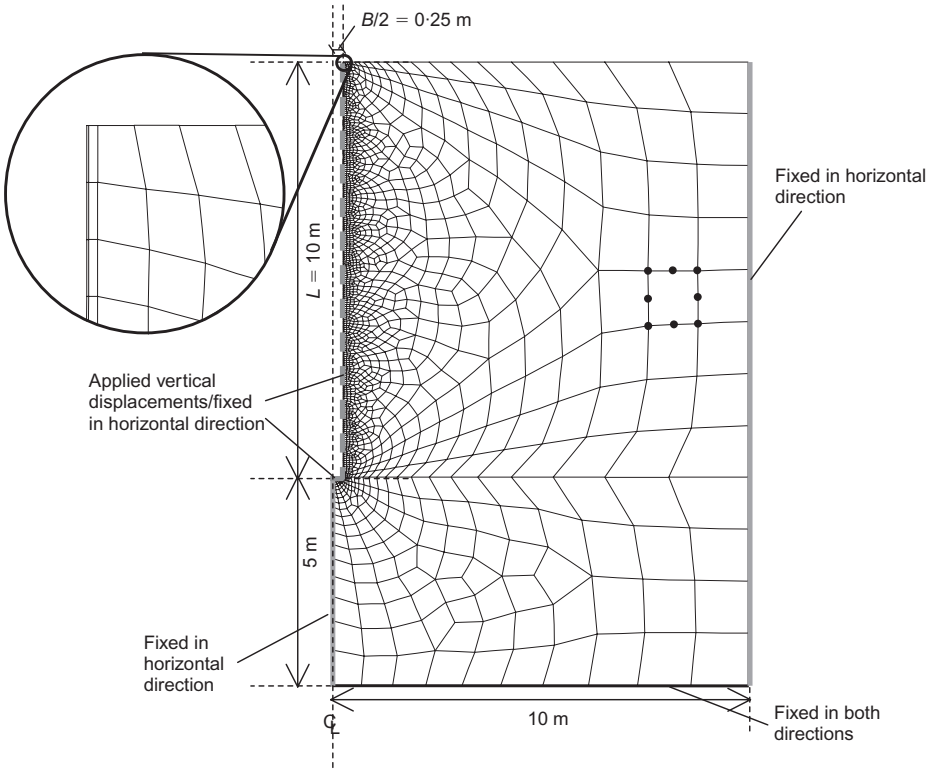

Fig. 6. Finite element mesh and boundary conditions in full pile simulations

during pile loading is observed to decrease with increasing K_0; however, for a normally consolidated sand (with K_0 in the 0·4 to 0·5 range) the change of K/K_0 due to oscillations of K_0 within this range can, for practical purposes, be neglected.

To check the sensitivity of the present analysis to the assumed value of the shear band thickness, some analyses were done with the size of the leftmost element t_s being $5D_{50}$ and $20D_{50}$. The value of K decreases with decreasing t_s, with the differences becoming larger for denser sand. Nevertheless, the differences never exceeded 6%, even for the densest sand (Fig. 10(a)). Loose sand ($D_R < 45\%$) appears to be particularly insensitive to the size of the leftmost element. This can be attributed to the fact that localisation at low densities is either limited or non-existent because of the significantly smaller tendency for dilation and softening. Fig. 10(b) shows results from simulations with $\sigma'_{v0} = 100$ kPa, $K_0 = 0{\cdot}4$, $t_s = 10D_{50}$ and pile diameter B ranging from 0·3 m to 1·5 m. We observe there is the tendency for K to decrease with increasing B, but the differences never exceeded 5%. Therefore, for the examined B range (which spans the range of most drilled shafts encountered in practice), the pile diameter has negligible effect.

It is interesting to note that analyses with different t_s and B values but with the same t_s/B ratio yield nearly identical results. Thus the effect of scale is totally controlled by the ratio t_s/B rather than by the absolute magnitude of either B or t_s. The dependence of the results on the ratio t_s/B is useful in assessing the difference between the values of K/K_0 for a prototype pile and a model pile installed in the same soil (any such difference can be referred to as 'scale effect'), a topic investigated experimentally by Foray *et al.* (1998), Garnier & König (1998) and Lehane *et al.* (2005), among others. The t_s/B values for the analysis presented in Fig. 10 are very small and comparable. K/K_0 is plotted against t_s/B for $D_R = 90\%$ and $\sigma'_{v0} = 100$ kPa in Fig. 11 with the addition of extra data points for large t_s/B values. Fig. 11 shows that scale effects are small when $t_s/B < 0{\cdot}01$ ($B/D_{50} > 1000$) but become important in model pile testing, for which t_s/B may be very large. According to Garnier & König (1998), grain size effects become negligible for B_m/D_{50} larger than 100, while Foray *et al.* (1998) suggest that they become insignificant for B_m/D_{50} larger than 200 (B_m is the diameter of the model pile). However, closer inspection of data on shear resistance plotted against B_m/D_{50} in Foray *et al.* (1998) and Garnier & König (1998) confirms that there is a notable tendency for the decrease in unit shaft resistance (soil shear strength along the soil/pile interface) to continue with further increase of B_m/D_{50} beyond the 100–200 ($t_s/B < 0{\cdot}05$–$0{\cdot}1$) range. By extrapolating to B_m/D_{50} values in the 1000–8000 range ($t_s/B < 0{\cdot}0012$–$0{\cdot}010$), which is applicable to full-scale piles, we see that there is significant potential for additional shear strength decrease.

Based on the one-dimensional simulation results (Fig. 9), we can propose the following equation for the value of K/K_0 in terms of D_R, σ'_{v0} and K_0:

$$\frac{K}{K_0} = \frac{1}{F(K_0)} C_1 \exp\left\{\frac{D_R}{100\%}\left[1{\cdot}3 - 0{\cdot}2\ln\left(\frac{\sigma'_{v0}}{p_A}\right)\right]\right\} \qquad (21)$$

for 50 kPa $\leqslant \sigma'_{v0} \leqslant$ 500 kPa and 30% $\leqslant D_R \leqslant$ 90% with $p_A = 100$ kPa or equivalent values in other units. D_R in equation (21) must be entered as a percentage (a number from 0% to 100%). $F(K_0)$ is a function that introduces the effect of K_0, and it is taken as $\exp[0{\cdot}2\sqrt{K_0 - 0{\cdot}4}]$. The constant C_1 takes the values of 0·71 and 0·63 for Toyoura sand and Ottawa sand respectively. An approximate value of 0·7 may be used for C_1 in calculations for clean sands. Equation (21) is based on results from simulations for only two clean sands: therefore its use in practical problems involving other sands, including sands with fines, requires further verification.

Two-dimensional analysis (analysis of a full pile)

For the two-dimensional axisymmetric analysis, we consider a 10 m long pile with $B = 0{\cdot}5$ m. The thickness of the

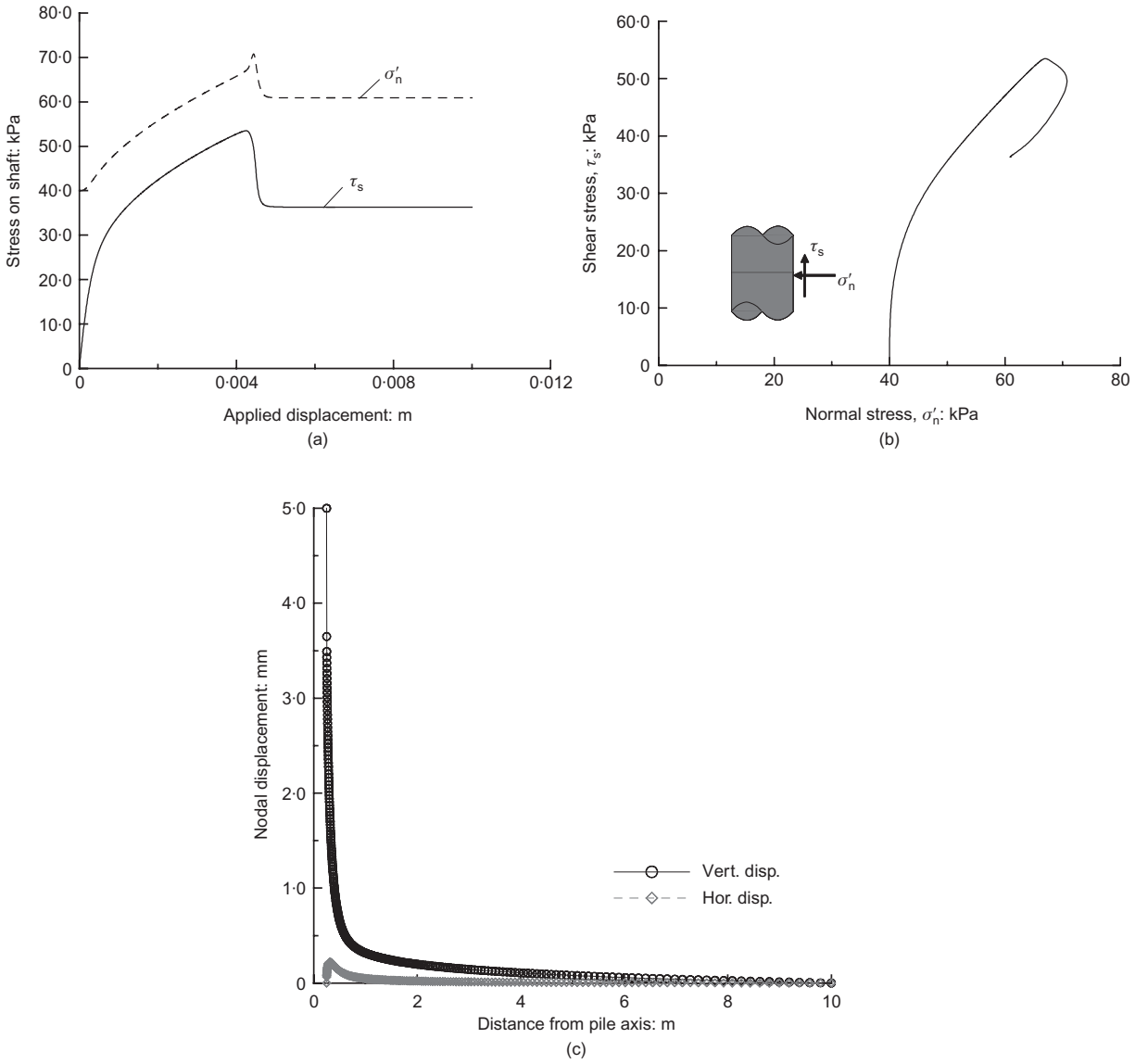

Fig. 7. (a) Stresses acting on shaft against displacement curves, (b) stress path, and (c) horizontal and vertical nodal displacements from analysis for Toyoura sand with $\sigma'_{v0} = 100$ kPa, $D_R = 60\%$, $K_0 = 0{\cdot}4$, $B = 0{\cdot}5$ m

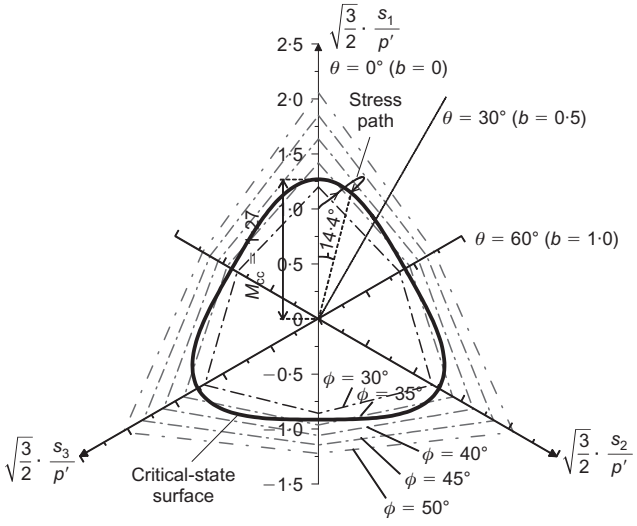

Fig. 8. Stress path in normalised deviatoric plane from analysis for Toyoura sand with $\sigma'_{v0} = 100$ kPa, $D_R = 60\%$, $K_0 = 0{\cdot}4$, $B = 0{\cdot}5$ m

elements adjacent to the boundary representing the pile shaft wall is set to $10D_{50}$. The mesh, shown in Fig. 6, contains 2004 elements and 6285 nodes. Fig. 12(a) shows the development of total shaft resistance Q_s against pile displacement. The evolution of the total normal reaction to the pile shaft against pile displacement is plotted in Fig. 12(b). Fig. 12(b) implies that the average increase in K/K_0 across the entire pile length at the state of limit shaft resistance mobilisation is 1·46 and 1·72 for simulations with $D_R = 45\%$ and $D_R = 60\%$ respectively. As in the one-dimensional simulations, the mobilised friction angle δ along the pile/soil contact is 30·8°. If we had considered a soil disc midway between the pile tip and the pile head, the K/K_0 values would have been 1·39 and 1·64 for $D_R = 45\%$ and $D_R = 60\%$, which are about 5% smaller than the two-dimensional predictions. The higher values of K/K_0 for the two-dimensional analysis result from the fact that, in the two-dimensional analyses, the pile has a finite length and, as a consequence, stresses are transmitted to soil located far from the shaft and lying below the elevation of the pile base (Fig. 5). Therefore, in two-dimensional analyses, the soil can better react to the pile settlement, thus increasing the total shaft resistance.

The shaft resistance is mobilised progressively (Fig.

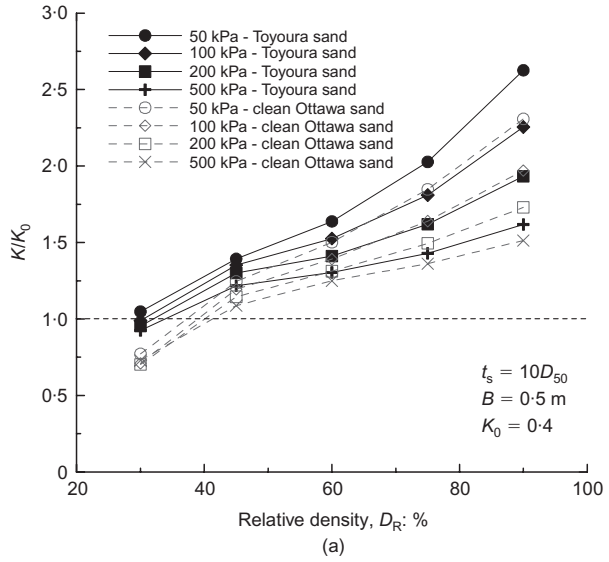

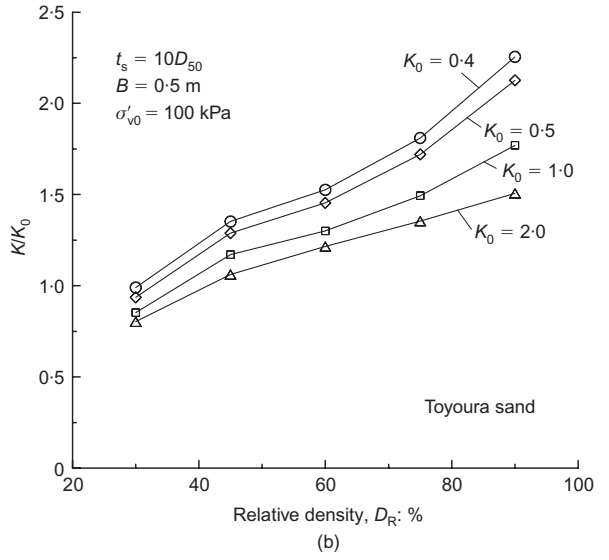

Fig. 9. Effect of (a) initial effective overburden stress and relative density and (b) coefficient of earth pressure at rest on K/K_0

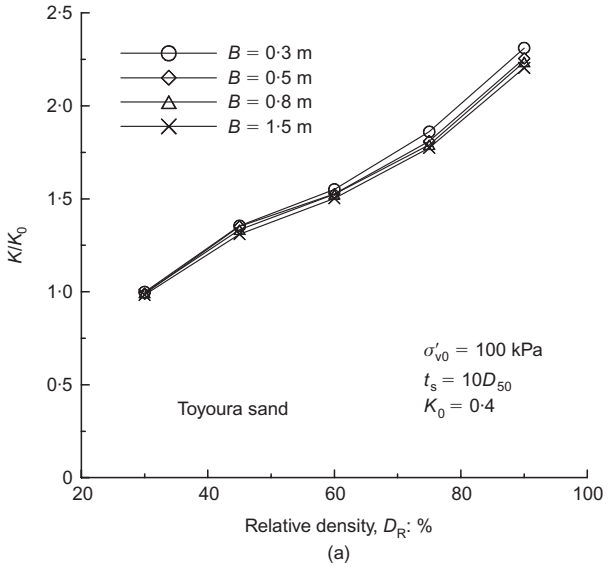

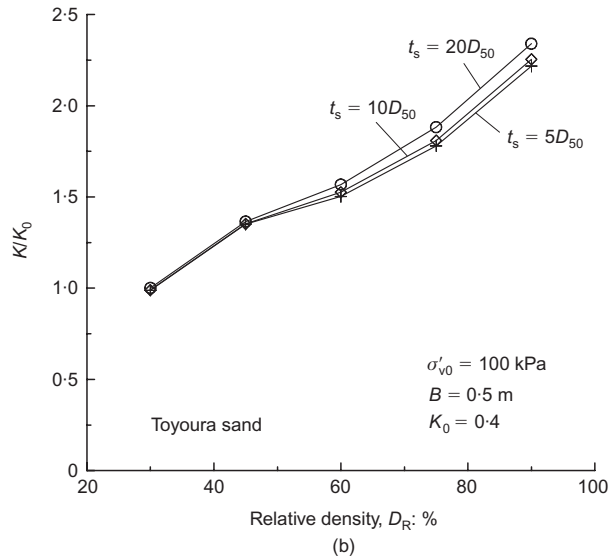

Fig. 10. Effect of (a) assumed shear band thickness t_s (size of leftmost element) and (b) pile diameter B on K/K_0

13(a)), starting from the top of the shaft (where the stress levels are smaller and the soil response exhibits a higher degree of softening) and propagating downwards. The progressive failure can also explain why the degree of brittleness exhibited in the global load–settlement response (Fig. 12) is smaller than that observed in one-dimensional simulations. The enhanced normal reaction in the two-dimensional analyses is counterbalanced to some extent by a loss of normal effective stress that occurs in the region approximately $2B$ above the pile tip (Fig. 13(a)). This is due to the interaction of the pile base movement and of the soil just above the pile base elevation. From Fig. 13(b), we see that, as in the one-dimensional analyses, the normal stress build-up for Ottawa sand is smaller than for Toyoura sand.

Let us now consider two analyses, one with soil unit weight $\gamma' = 10$ kN/m^3 (case I) and one with $\gamma' = 20$ kN/m^3 (case II). The choice of the two unit weights allows us to obtain estimates of K/K_0 at the same depth but with values of σ'_{v0} that differ by a factor of 2. The profiles of K/K_0 yielded by the two-dimensional axisymmetric analyses are compared with values originating from the one-dimensional simulations (Fig. 14). The difference between the results from the one-dimensional and two-dimensional analyses

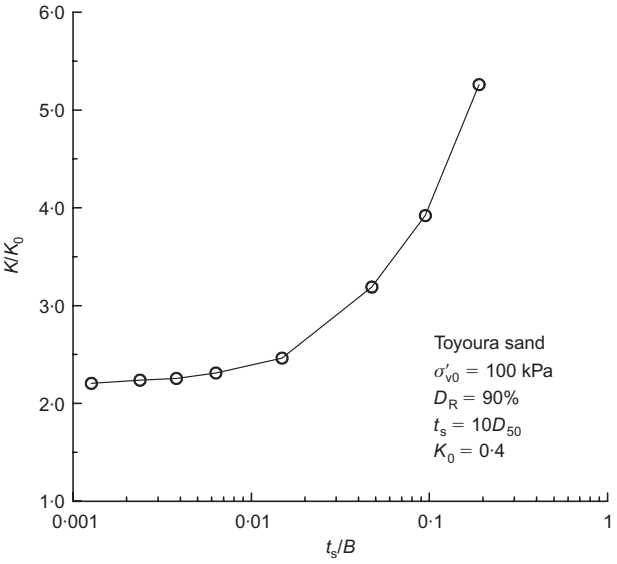

Fig. 11. Scale effect: K/K_0 from analyses with different t_s/B ratio

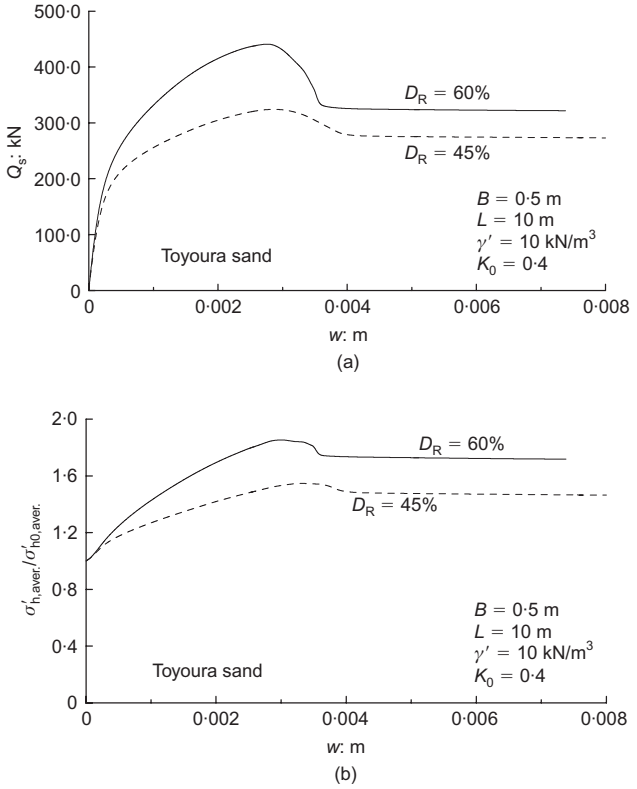

Fig. 12. (a) Shaft resistance against pile displacement; (b) evolution of average normal stress acting on shaft with pile displacement

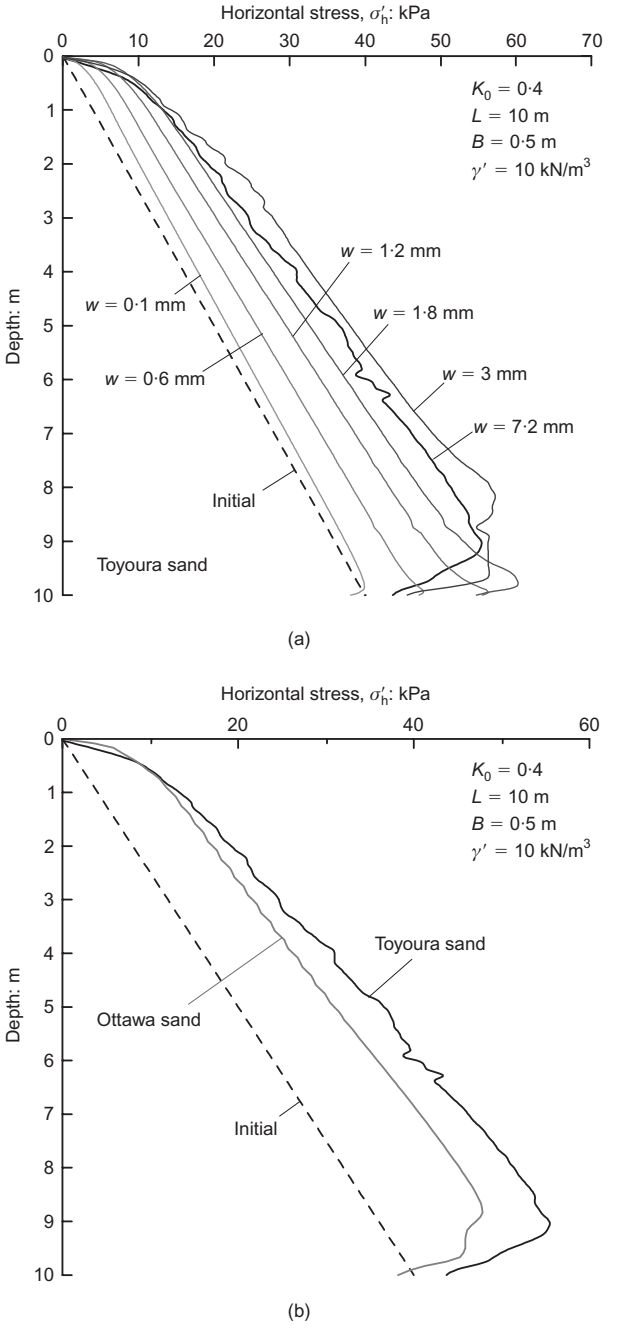

Fig. 13. (a) Profiles of lateral effective stress acting along pile shaft at several stages of pile settlement; (b) profiles of lateral effective stress at stage of full mobilisation of shaft resistance

becomes larger closer to the ground surface. However, the effect of such differences on the predicted total shaft resistance is small because the stresses close to the ground surface are generally small. For example, if we use equation (21) to obtain q_{sL} along the entire pile length, and then integrate to get Q_s for the two example cases I and II shown in Fig. 14, the resulting Q_s is only 5–6% lower than the one resulting from the two-dimensional simulations. These numbers apply to the present simulations of a 10 m long drilled shaft; for longer piles, the conditions resemble those of the one-dimensional analysis over a larger fraction of the pile length, rendering the differences between the one-dimensional and two-dimensional predictions negligible. Therefore results based on one-dimensional analysis may be used to estimate K for pile design.

A final factor to consider is pile deformability (often referred to in the literature as 'Poisson's effect'). So far, we have considered a pile that is perfectly rigid. In reality, an increase in the axial load leads to axial contraction of the drilled shaft, which in turn leads to an increase in B that is controlled by the Poisson's ratio of the concrete. This lateral expansion of the drilled shaft is very small and leads only to a marginal increase of the normal effective stress on the shaft. Analyses with the pile included in the mesh ($E_{pile} = 21$ GPa and $\nu_{pile} = 0{\cdot}2$), with prescribed displacements applied at the pile head, yield Q_{sL} that is only 1·5% greater than that obtained from the original rigid pile analyses. The contraction of the pile has a more pronounced effect on the settlement required for shaft capacity mobilisation. The analyses with a deformable pile show that the shaft resistance develops more gradually, with Q_{sL} mobilised at head displacements that are 25% greater than for a rigid pile (because of the shortening of the pile as the axial load increases). The fact that the Poisson's effect on the limit shaft capacity of the drilled shafts is very small is also evident from the analytical equations and plots based on numerical results presented by De Nicola & Randolph (1993) if the input parameters take values that are typical for drilled shafts.

Comparison with experimental results

Data from experimental and field studies published in the literature support the notion that the value of K for dense sand and low confinement can be much greater than K_0. Touma & Reese (1974) and Reese *et al.* (1976) performed a series of instrumented pile load tests. According to these studies, the average K across the portion of the pile that is embedded in sand can be taken as 0·7 if the pile is not embedded more than 8 m in sand and as 0·5–0·6 if the pile embedment in sand is larger. It appears that the results of the present FE analysis are largely in agreement with these

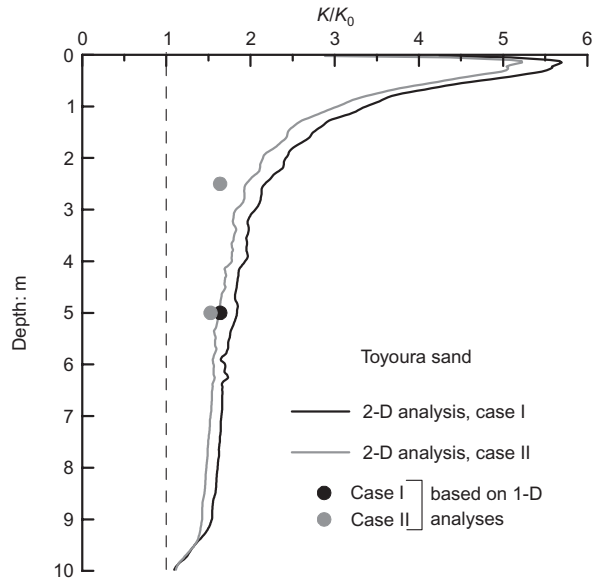

Fig. 14. Profiles of ratio K/K_0 from two-dimensional axisymmetric analyses at stage of limit shaft resistance mobilisation

numbers for the usual range of soil densities and levels of effective overburden stress encountered in drilled shaft (bored pile) designs. The Reese & O'Neill (1988) design equation ($\beta = 1{\cdot}5 - 0{\cdot}245z^{0{\cdot}5}$ with $0{\cdot}25 \leqslant \beta \leqslant 1{\cdot}2$, for $N_{SPT} \geqslant 15$) reflects conditions of the sandy formations of the Texas Gulf Coast region, which, according to O'Neill & Hassan (1994), are overconsolidated and aged. The K_0 value considered by O'Neill & Hassan (1994) at depths larger than 15 m appears to be of the order of 0·8. Using our numerical results and considering $K_0 = 0{\cdot}8$, we predict β in the range 0·6–1·25 for sand ranging from medium dense at 20 m depth to dense sand at 2 m depth; these values are in good agreement with the Reese & O' Neill (1988) equation.

Lehane *et al.* (1993) performed field load tests on instrumented piles that were installed in loose to medium dense sand using jacking (displacement piles). Their data show that the radial effective stress acting on the pile shaft at peak resistance conditions during the load test was 1·3 to 1·7 times higher than the one recorded after installation. In the case of displacement piles: (a) the density and stress state of the soil in the vicinity of the shaft change during pile installation from their original in situ values; and (b) the soil density and the stress state at the start of the pile loading are not uniform (varying predominantly in the radial direction). Setting aside these two deviations with respect to the non-displacement piles we modelled, the Lehane *et al.* (1993) tests provide evidence that the radial stress increase during axial loading can be significant even in medium dense sand.

Fioravante (2002) and Colombi (2005) present data from model tests of non-displacement piles performed in a centrifuge. Some of the tests involved model piles with high relative roughness ($R_n = 0{\cdot}45$) embedded in Toyoura sand with $D_R \approx 90\%$ and 66%. Relative roughness R_n is the ratio of the absolute roughness R_{max}, expressing the maximum asperity height measured over a specific length L_R (usually $= D_{50}$) along the frictional interface, to the D_{50} of the sand. For such a high value of R_n, failure occurs inside the soil mass surrounding the shaft rather than between pile shaft and soil (Uesugi *et al.*, 1988; Lings & Dietz, 2005), as in the case of a drilled shaft. Taking into account that the residual friction coefficient of Toyoura sand in direct interface simple shear tests with high interface roughness is around 0·6 (Uesugi *et al.*, 1988), the Fioravante (2002) data suggest that the value of K for bored piles in very dense sand can be in the range of 1·2 to 3·7, with the higher values corresponding to shallower depths (lower confining stresses).

It is well known that, although centrifuge testing achieves the establishment in small-scale models of a stress field and stress gradients that are representative of real ground conditions, the relatively large size of the sand grains with respect to the model pile diameter is in contrast with prototype conditions. For the diameter of model piles, which is usually of the order of a few centimetres, even fine sand would correspond to gravel-size material in prototype scale. Since the shear band developing along the pile shaft is independent of the centrifuge acceleration and is of the order of $10D_{50}$, the shear band thickness t_s is a non-negligible fraction of the model pile diameter B_m. Such large values of t_s/B_m produce excessively large values of K, as shown in an earlier section.

We may attempt an interpretation of centrifuge tests presented by Fioravante (2002) and Colombi (2005) by using FE modelling and the soil-disc approach. In these tests, the diameter of the model piles was 10 mm, which represented a prototype pile in the field with a diameter of 0·8 m (applied centrifuge acceleration 80g). For the case of Toyoura sand, the ratio of the model pile diameter B_m (= 10 mm) to D_{50} is approximately 53: thus the size of the leftmost element is set to $0{\cdot}19B$ ($= 10D_{50}B/B_m$). A comparison between the response from analyses with $t_s/B = 0{\cdot}0024$ ($t_s = 10D_{50} = 1{\cdot}9$ mm) and $t_s/B = 0{\cdot}19$ ($t_s = 152$ mm) is made in Fig. 15. As expected, there is a very large contrast between the

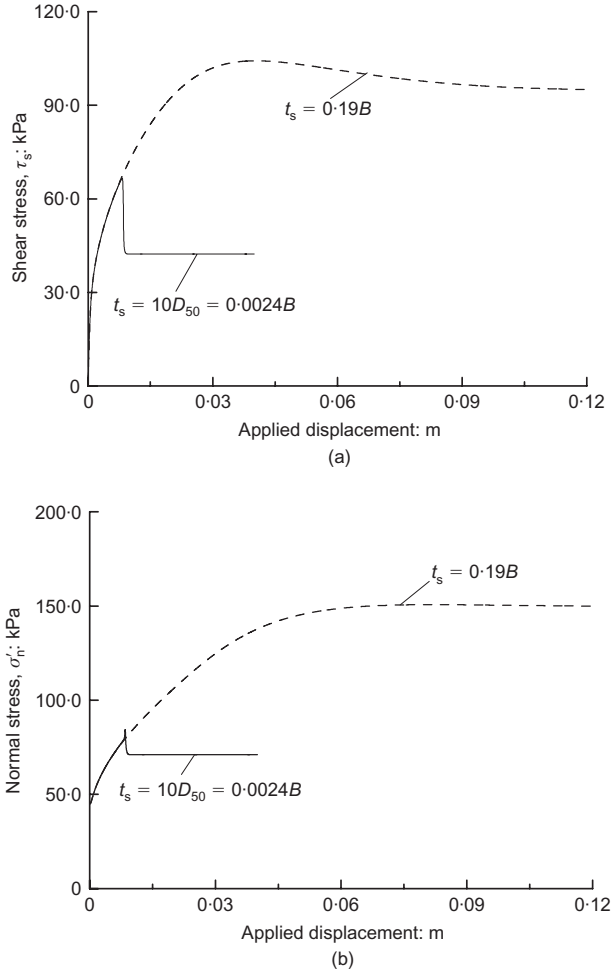

Fig. 15. (a) Shear stress and (b) effective normal stress acting on shaft against displacement from analyses for Toyoura sand with $\sigma'_{v0} = 100$ kPa, $D_R = 66\%$, $K_0 = 0{\cdot}45$, $B = 0{\cdot}8$ m

stresses mobilised, reflecting a strong influence of scale. Moreover, the analysis with $t_s/B = 0{\cdot}19$, which represents the shear band thickness in the centrifuge tests, is much less brittle than the response of the analysis with realistic t_s values at prototype scale. Another interesting fact about the analysis with large t_s is that the mobilised friction angle δ is not $30{\cdot}8^\circ$ ($\mu = 0{\cdot}60$), as observed for the prototype, but $32{\cdot}3^\circ$ ($\mu = 0{\cdot}63$). This deviation is because, as the element representing the shear band becomes larger, the distance of the stress computation points (Gauss quadrature points) from the pile shaft also increases.

A comparison is made in Fig. 16 between the FE predictions of β and the centrifuge data (Fioravante, 2002; Colombi, 2005). It can be seen that the analyses with $t_s/B = 0{\cdot}19$ (solid lines) are in fair agreement with the centrifuge data, in contrast to the analyses with $t_s/B = 0{\cdot}0024$. As expected, the shaft resistance that the prototype would have developed (obtained using a realistic shear band thickness $t_s = 0{\cdot}0024B$ and shown in the figure as a dashed line) is much smaller than that observed in centrifuge tests and in the simulations with $t_s/B = 0{\cdot}19$ (solid lines). It is interesting to note that, for the same centrifuge tests on dense Toyoura sand ($D_R = 90\%$) and $\sigma'_{h0} = 55$ kPa, Lehane *et al.* (2005) predicted, using an approach based on a cavity expansion analogue, that the K/K_0 of the prototype pile ought to be only 0·34 times that measured in the model test. According to our simulations, this number is around 0·42.

SUMMARY AND CONCLUSIONS

We conducted a numerical study of the factors affecting the limit shaft resistance of non-displacement piles with the aid of advanced constitutive modelling that captures the effects of fabric-induced cross-anisotropy and of the intermediate principal stress. Based on the results of the numerical analysis, we can draw the following conclusions.

(*a*) The coefficient of lateral pressure K at full mobilisation of limit shaft resistance increases with increasing sand relative density and decreases with increasing initial effective overburden stress. For a loose sand, K will be approximately equal to K_0, while it may be greater than 1 for high relative densities and low confining stresses, even if the sand is normally consolidated.

(*b*) The K/K_0 ratio decreases with increasing K_0, suggesting that the lateral stress build-up would be less intense in the case of an overconsolidated sand.

(*c*) The value of K increases with decreasing pile diameter. However, this effect is small to negligible for the range of pile diameters and grain sizes usually encountered in practice. The effect of scale becomes an important issue in model pile testing in laboratory studies, in which the ratio of mean grain size to the model pile diameter is relatively large.

(*d*) The friction angle δ mobilised along the pile shaft is independent of relative density and effective stress level. For design purposes, it can be taken as $0{\cdot}95\phi_c^{TXC}$ to ϕ_c^{TXC}, where ϕ_c^{TXC} is the critical-state friction angle in triaxial compression.

(*e*) Despite the fact that the soil disc simulations (one-dimensional axisymmetric) generally underpredict the value of K that develops in two-dimensional axisymmetric conditions, the K estimates based on one-dimensional simulations constitute good approximations of the real values for points not lying excessively close to the ground surface (which essentially control the total shaft resistance) and can be used for the determination of the shaft resistance Q_s.

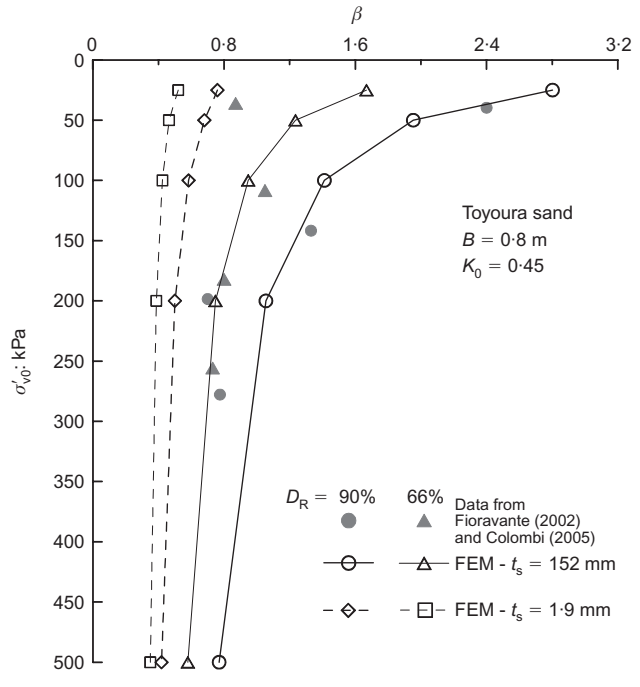

Fig. 16. Values of β against effective overburden stress from soil disc simulations with $t_s = 10D_{50} = 1{\cdot}9$ mm as well as $t_s = 0{\cdot}19B = 152$ mm compared with centrifuge test data

ACKNOWLEDGEMENTS

The financial support provided to the first author by the Alexander S. Onassis Public Benefit Foundation is gratefully acknowledged. Motivation to research the dependence of unit shaft resistance of drilled shafts on soil state resulted from discussions with Monica Prezzi.

REFERENCES

Abbo, A. J. & Sloan, S. W. (2000). *SNAC, User manual, Version 2·0*. Department of Civil, Surveying and Environmental Engineering, University of Newcastle, Callaghan, Australia.

Boulon, M. & Foray, P. (1986). Physical and numerical simulation of lateral shaft friction along offshore piles in sand. *Proc. 3rd Int. Conf. Numerical Methods in Offshore Piling, Nantes*, 127–147.

Carraro, J. A. H. (2004). *Mechanical behavior of silty and clayey sands*. PhD dissertation, Purdue University.

Carraro, J. A. H., Bandini, P. & Salgado, R. (2003). Liquefaction resistance of clean and nonplastic silty sands based on cone penetration resistance. *J. Geotech. Geoenviron. Engng, ASCE* **129**, No. 11, 965–976.

Colombi, A. (2005). *Physical modeling of an isolated pile in coarse grained soils*. PhD dissertation, University of Ferrara.

Dafalias, Y. F. & Manzari, M. T. (2004). Simple plasticity sand model accounting for fabric change effects. *J. Engng Mech.* ASCE **130**, No. 6, 622–634.

Dafalias, Y. F., Papadimitriou, A. G. & Li, X. S. (2004). Sand plasticity model accounting for inherent fabric anisotropy. *J. Engng Mech.* ASCE **130**, No. 11, 1319–1333.

De Nicola, A. & Randolph, M. F. (1993). Tensile and compressive shaft capacity of piles in sand. *J. Geotech. Engng, ASCE* **119**, 12, 1952–1973.

Fioravante, V. (2002). On the shaft friction modeling of non-displacement piles in sand. *Soils Found.* **42**, No. 2, 23–33.

Fleming, W. G. K., Weltman, A. J., Randolph, M. F. & Elson W. K. (1992). *Piling Engineering*, 2nd edn. New York: John Wiley & Sons.

Foray, P., Balachowski, L. & Rault, G. (1998). Scale effect in shaft friction due to the localisation of deformations. *Centrifuge 98*

(Kimura, T., Kusakabe, O. and Takemura, J. (eds)), pp. 211–216. Rotterdam: Balkema.

Fukushima, S. & Tatsuoka, F. (1984). Strength and deformation characteristics of saturated sand at extremely low pressures. *Soils Found.* **24**, No. 4, 30–48.

Garnier, J. & König, D. (1998). Scale effects in piles and nails loading tests in sand. *Centrifuge 98* (Kimura, Kusakabe & Takemura, eds), 205–210. Rotterdam: Balkema.

Gens, A. & Potts, D. M. (1984). Formulation of quasi-axisymmetric boundary value problems for finite element analysis. *Engng Comput.* **1**, No. 2, 144–150.

Ghionna, V. N. & Mortara, G. (2002). An elastoplastic model for sand-structure interface behaviour. *Géotechnique* **52**, No. 1, 41–50.

Hardin, B. O. & Richart, F. E. Jr (1963). Elastic wave velocities in granular soils. *J. Soil Mech. Found. Div. ASCE* **89**, No. SM1, 33–65.

Lam, W.-K. & Tatsuoka, F. (1988). Effects of initial anisotropic fabric and σ_2 on strength and deformation characteristics of sand. *Soils Found.* **28**, No. 1, 89–106.

Lehane, B. M., Jardine, R. J., Bond, A. J. & Frank, R. (1993). Mechanisms of shaft friction in sand from instrumented pile tests. *J. Geotech. Engng, ASCE* **119**, No. 1, 19–35.

Lehane, B. M., Gaudin, C. & Schneider, J. A. (2005). Scale effects on tension capacity for rough piles buried in dense sand. *Géotechnique* **55**, No. 10, 709–719.

Li, X. S. & Dafalias, Y. F. (2000). Dilatancy of cohesionless soils. *Géotechnique* **50**, No. 4, 449–460.

Li, X. S., Dafalias, Y. F. & Wang, Z. L. (1999). State-dependent dilaltancy in critical state constitutive modeling of sand. *Can. Geotech. J.* **36**, No. 4, 599–611.

Lings, M. L. & Dietz, M. S. (2005). The peak strength of sand-steel interfaces and the role of dilation. *Soils Found.* **45**, No. 6, 1–14.

Loukidis, D. (2006). *Advanced constitutive modeling of sands and applications to foundation engineering.* PhD dissertation, Purdue University.

Loukidis, D. & Salgado, R. (2008). Modeling sand response using two-surface plasticity. *Comput. Geotech.* (in press).

Manzari, M. & Dafalias, Y. (1997). A critical state two-surface plasticity model for sands. *Géotechnique* **47**, No. 2, 255–272.

Mesri, G. & Hayat, T. M. (1993). The coefficient of earth pressure at rest. *Can. Geotech. J.* **30**, No. 4, 647–666.

Murthy, T. G., Loukidis, D., Carraro, J. A. H, Prezzi, M. & Salgado, R. (2006). Undrained monotonic behavior of clean and non-plastic silty sands. *Géotechnique* **57**, No. 3, 273–288.

Nemat-Nasser, S. & Okada, N. (2001). Radiographic and microscopic observation of shear bands in granular materials. *Géotechnique* **51**, No. 9, 753–765.

O' Neill, M. W. & Hassan, K. M. (1994). Drilled shafts: effects of construction on performance and design criteria. *Proceedings of the international conference on design and construction of deep foundations*, Orlando, pp. 137–187.

Papadimitriou, A. G. & Bouckovalas, G. D. (2002). Plasticity model for sand under small and large cyclic strains: a multiaxial formulation. *Soil Dynam. Earthquake Engng* **22**, No. 3, 191–204.

Potts, D. M. & Martins, J. P. (1982). The shaft resistance of axially loaded piles in clay. *Géotechnique* **32**, No. 4, 369–386.

Potts, D. M. & Zdravković L. (1999). *Finite element analysis in geotechnical engineering: Theory.* London: Thomas Telford.

Pradhan, B. S., Tatsuoka, F. & Horii, N. (1988). Strength and deformation characteristics of sand in torsional simple shear. *Soils Found.* **28**, No. 3, 131–148.

Reese, L. C. & O' Neill, M. W. (1988). *Drilled shafts: Construction procedures and design methods*, Publication No. FHWA-HI-88-042. Washington, DC: Federal Highway Administration.

Reese, L. C., Touma, F. T. & O'Neill, M. W. (1976). Behavior of drilled piers under axial loading. *J. Geotech. Engng Div. ASCE* **102**, No. GT5, 493–510.

Salgado, R. (2006). The role of analysis in non-displacement pile design. In *Modern trends in geomechanics*, Springer Proceedings in Physics, Vol. 106 (eds W. Wu and H.-S. Yu), pp. 521–540. Berlin: Springer.

Salgado, R. (2008). *The engineering of foundations*. New York: McGraw-Hill.

Sloan, S. W. & Booker, J. R (1992). Integration of Tresca and Mohr–Coulomb constitutive relations in plane strain elastoplasticity. *Int. J. Numer. Methods Engng* **33**, No. 1, 163–196.

Tabucanon, J. T., Airey, D. W. & Poulos, H. G. (1995). Pile skin friction in sands from constant normal stiffness tests. *Geotech. Test. J.* **18**, No. 3, 350–364.

Touma, F. T. & Reese, L. C. (1974). Behavior of bored piles in sand. *J. Geotech. Engng Div. ASCE* **100**, No. GT7, 749–761.

Uesugi, M., Kishida, H. & Tsubakihara, Y (1988). Behavior of sand particles in sand-steel friction. *Soils Found.* **28**, No. 1, 107–118.

Uesugi, M. , Kishida, H. & Uchikawa, Y. (1990). Friction between dry sand and concrete under monotonic and repeated loading. *Soils Found.* **30**, No. 1, 115–128.

Vardoulakis, I. & Sulem, J. (1995). *Bifurcation analysis in geomechanics*. London: Blackie Academic and Professional.

Yoshimine, M., Ishihara, K. & Vargas, W. (1998). Effects of principal stress direction and intermediate principal stress on undrained shear behavior of sand. *Soils Found.* **38**, No. 3, 179–188.